Supplementary Information (SI) for Journal of Materials Chemistry A.

Oxidized Covalent Organic Frameworks with Enhanced Local Polarization for Superior Photocatalytic Production of Hydrogen Peroxide

Huaji Pang[a], Mengna Tan[a], Tao Guo[a], Zhiguo Zhang[b], Yanqiu Zhu[a], Chizhu Ding[a], Mingkui Wang[b], Yonggang Xiang[a], Dekang Huang[a]**

[a]College of Chemistry, Huazhong Agricultural University, Wuhan 430070, PR China

[b]Wuhan National Laboratory for Optoelectronics, Huazhong University of Science and Technology, Wuhan 430074, China

E-mail: dingchizhu@mail.hzau.edu.cn (C. Ding), huangdekang@mail.hzau.edu.cn (D. Huang)

Table of Contents

1. General information

1.1 Chemicals

Unless otherwise stated, all the chemicals were purchased in analytical purity from commercial suppliers and used directly without further purification.

1.2 Characterization methods

Powder X-ray diffraction (PXRD) patterns were collected on a Bruker D8 Advance diffractometer with Cu Kα radiation (2θ range: 2-40°; Scan step size: 0.02°; Time per step: 1 s). Fourier transform infrared (FT-IR) spectra were obtained using a Nicolet 6700 spectrometer (Thermo Scientific, USA) equipped with an ATR cell. The specific Brunauer-Emmett-Teller (BET) surface area and pore size distribution were recorded at 77 K with a Micromeritics ASAP 2040 instrument. Transmission electron microscopy (TEM) images were acquired using a Talos F200x instrument at an accelerating voltage of 200 kV. Scanning electron microscopy (SEM) images were acquired using a Hitachi SU 8010 microscope. X-ray photoelectron spectroscopy (XPS) measurements were conducted on a Thermo ESCALAB 250XI spectrometer using non-monochromatic Al Kα X-rays as the excitation source, with C 1s (284.6 eV) as the reference line. Solid-state diffuse reflectance Ultraviolet–visible (UV-vis) spectra were acquired using a Perkin-Elmer LAMBDA 650S spectrophotometer with $BaSO_4$ as the reference. Photoluminescence (PL) spectra were recorded on a Shimadzu RF-5301PC spectrophotometer. Photoluminescence lifetime was measured using the time-correlated single photon counting method (FluoTime 250, Germany). Free radicals were tested by the Electron paramagnetic resonance (EPR) spectrometer (MS5000X,

Bruker, UK). In situ infrared spectra were obtained using diffuse reflectance infrared fourier transform spectroscopy (DRIFTS) (Nicolet iS50, Thermo Scientific, USA). Temperature-dependent photoluminescence spectra were recorded on a Fluorolog QM spectrophotometer (Horiba, Japan) over a temperature range from 80 to 300 K with an excitation wavelength (λ_{ex}) of 375 nm. The concentrations of FF and FA were analyzed by the high-performance liquid chromatography (HPLC) (Agilent 1290 Infinity II HDR-DAD).

1.3 Electrochemical measurements

Electrochemical measurements were carried out with a CHI 760E workstation (Chenhua Instruments, China) using a standard three-electrode system. Typically, 15 mg of COFs, 1 mL of isopropanol and 50 μL of 5% Nafion solution were mixed together, and 200 μL of this mixture was coated on a ITO glass (10 × 15 × 1.1 mm), which was employed as the working electrodes. Pt plate was utilized as the counter electrode and Ag/AgCl electrode as the reference electrode. 0.1 M Na_2SO_4 aqueous solution was employed as the electrolyte for the photocurrent test, while the aqueous solution of 0.1 M KCl and 0.005 M $K_3[Fe(CN)_6]$ was employed as the electrolyte for the electrochemical impedance spectroscopy (EIS) measurement. For Mott-Schottky tests, the perturbation was set to be 5 mV with frequencies of 1000, 2000, and 3000 Hz.

Rotating ring-disk electrode (RRDE) tests were also performed on the CHI 760E workstation (Chenhua Instruments, China), and the standard three-electrode system included a platinum plate as the counter electrode, a commercial Hg/HgO electrode as the reference electrode, and a catalyst-coated glassy carbon as the working electrode.

0.1 M KOH aqueous solution was employed as the electrolyte. RRDE tests were carried out at a scan rate of 10 mV s^{-1} and a rotation rate of 1600 rpm, and the ring potential was set to be 0.7 V (vs. Hg/HgO). All potentials versus Hg/HgO were calibrated to reversible hydrogen electrode (RHE) according to the following equation: *E* (vs. RHE) = *E* (vs. Hg/HgO) + 0.098 V + 0.059 V × pH. Hydrogen peroxide selectivity and electron transfer number (n) were calculated according to the following equations:

$$n = \frac{|4i_d|}{|i_d| + \frac{i_r}{N}}$$

$$H_2O_2(\%) = \frac{200i_r}{N|i_d| + i_r}$$

Where i_d is the disk current, i_r is the ring current, and N (0.37) is the collection efficiency.

1.4 Photocatalytic reaction

The photocatalytic production of H_2O_2 and FA was performed in a 50 mL double-shelled glass bottle at room temperature and under atmospheric pressure. The light source was a 300 W Xenon lamp (λ > 420 nm, PLS-SXE300D, Beijing Perfectlight, China). In a typical photocatalytic reaction, 10 mg of photocatalyst was suspended in an 11.6 mM FFA aqueous solution. Before illumination, the suspension was bubbled with O_2 for 30 mins to ensure O_2 saturation. After one hour reaction, 1 mL of solution was extracted. Then, the concentration of H_2O_2 was determined by adding 1 mL of 0.1 mol L^{-1} potassium hydrogen phthalate ($C_8H_5KO_4$) aqueous solution and 1 mL of 0.4 mol L^{-1} potassium iodide (KI) aqueous solution. In acidic conditions, the H_2O_2 generated oxidized the iodide anions to triiodide anions. This resulted in a strong

absorption peak at around 350 nm, which was observable with an ultraviolet spectrophotometer (UH5300, Japan).

1.5 Measurement of AQY and SCC

The apparent quantum yield (AQY) of the photocatalyst was measured under the irradiation of a 300 W Xeon lamp (PLS-SXE300D, Beijing Perfectlight, China) equipped with different band-pass filter. The average value of monochromatic light intensity at three representative points was obtained by PL-MW2000 optical radiometer. AQY were calculated according to the following equations:

$$\mathrm{AQY} = \frac{(\text{Number of produced H2O2 molecules}) * 2}{\text{Number of incident photons}} * 100\%$$

$$\mathrm{AQY} = \frac{(M\mathrm{H2O2} * NA * h * c) * 2}{S * P * T * \lambda} * 100\%$$

Where M = Yield of H_2O_2 (mol)

N_A (Avogadro constant) = $6.02*10^{23}$ mol^{-1}

h (Planck constant) = $6.626*10^{-34}$ J · s

c (Speed of light) = $3*10^8$ m/s

S = Irradiation area (cm^2) = 2.0 cm^2

P = the intensity of irradiation light (W/cm^2) = 13.6 mW/cm^2 (420 nm)

T = the photoreaction time (s) = 3600 s

λ = the wavelength of the monochromatic light (nm) = $420*10^{-9}$ m

The solar-to-chemical energy conversion (SCC) efficiency was determined by the photocatalytic experiments using a 300 W Xenon lamp (PLS-SXE300D, Beijing

Perfectlight, China) equipped with a 420 nm band-pass filter. The SCC efficiency was calculated according to the following equations:

$$\text{SCC}\ (\%) = \frac{[\ \triangle\ G \text{ for H2O2 formation } (\text{J mol}^{-1})] * [\text{H2O2 formed (mol)}]}{[\text{Total input power (W)}] * [\text{Reaction time (s)}]} * 100\%$$

Where $\triangle G$ was 117 kJ mol^{-1}, the light power intensity was 13.6 mW cm^{-2}, the irradiation area was 2.0 cm^{-2}, and the irradiation time was 3600 s.

1.6 Theoretical computation details

The first principles computations were carried out by Vienna Ab initio Simulation Package (VASP) based on density functional theory. Generalized gradient approximation (GGA) with the Perdew-Burke-Ernzerhof (PBE) functional was used to describe the exchange-correlation interaction. The projector augmented wave pseudopotentials were adopted to describe the ion-electron with a cutoff energy of 500 eV. The electronic energy and forces were converged to within 10^{-5} eV and 0.03 eVÅ-1, respectively. For the DFT calculations, the free energies of species were calculated as: $G = E_{DFT} + E_{ZPE} - T\Delta S$, where E_{DFT} was obtained from DFT energy, E_{ZPE} and $T\Delta S$ of adsorbed species were calculated by vibration analysis, whereas the thermodynamic corrections for gas molecules were from standard database.

2. Synthetic procedures

2.1 Synthesis of NQ-COF$_{S1}$

A Pyrex glass tube (10 mL) was charged with benzo[1,2-b:3,4-b':5,6-b"]trithiophene-2,5,8-tricarbaldehyde (33 mg, 0.10 mmol), 1,3,5-tris(4-aminophenyl)benzene (35 mg, 0.10 mmol), 1,3-dioxol-2-one (36 μL), $MgSO_4$ (72 mg), $[Cp^*RhCl_2]_2$ (5 mg), *o*-dichlorobenzene (1.0 mL), and acetic acid (50 μL).

Subsequently, the tube was sonicated for 10 minutes, degassed by three freeze-pump-thaw cycles (liquid nitrogen), and sealed under vacuum. After being heated in an oven at 120 °C for 3 days, the cooled suspension was centrifuged to separate the solid, which was repeatedly washed by tetrahydrofuran (THF), MeOH, and water until the solvent was colorless. The **NQ-COF$_{S1}$** was finally obtained as a sepia powder after being dried under vacuum at 80 °C.

2.2 Synthesis of NQ-COF$_{S1}$-O

A 10 mL Schlenk pressure tube was charged with **NQ-COF$_{S1}$** (35.2 mg, 0.05 mmol theoretical content of quinoline linkage), *m*-CPBA (51.8 mg, 0.3 mmol), and dichloromethane (DCM, 3.0 mL). Subsequently, the reaction mixture was stirred at 0 ℃ for 1 h, and then reacted at room temperature for 12 h. The solid was separated by filtration under reduced pressure, and washed with distilled water, THF, and DCM successively. Finally, **NQ-COF$_{S1}$-O** (33.7 mg) was obtained as a red brown powder after being dried under vacuum at 80 ℃.

3. Characterization

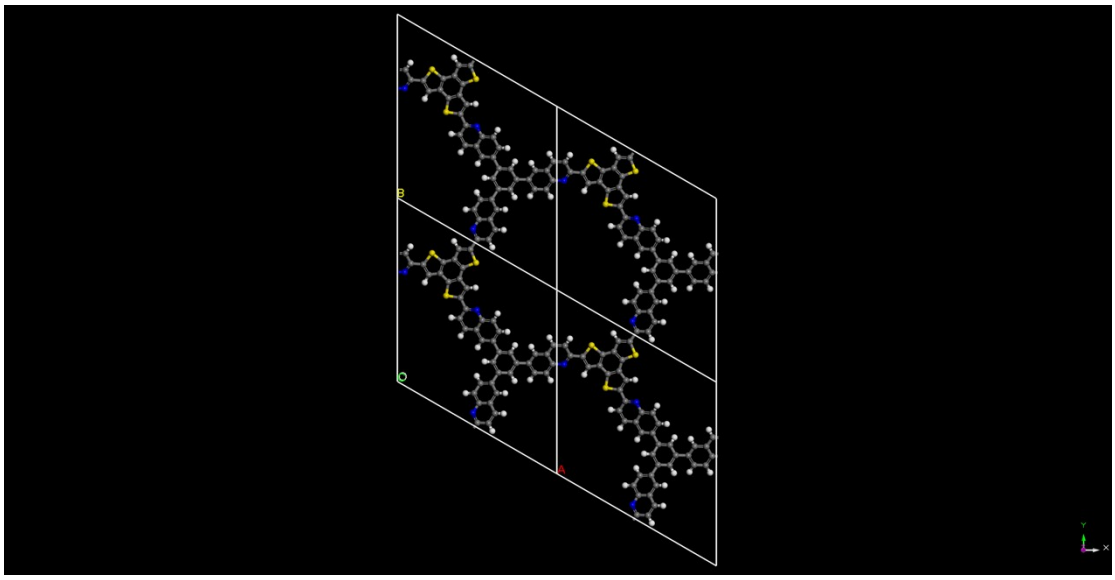

Fig. S1 AA-stacking structure of NQ-COF_{S1}.

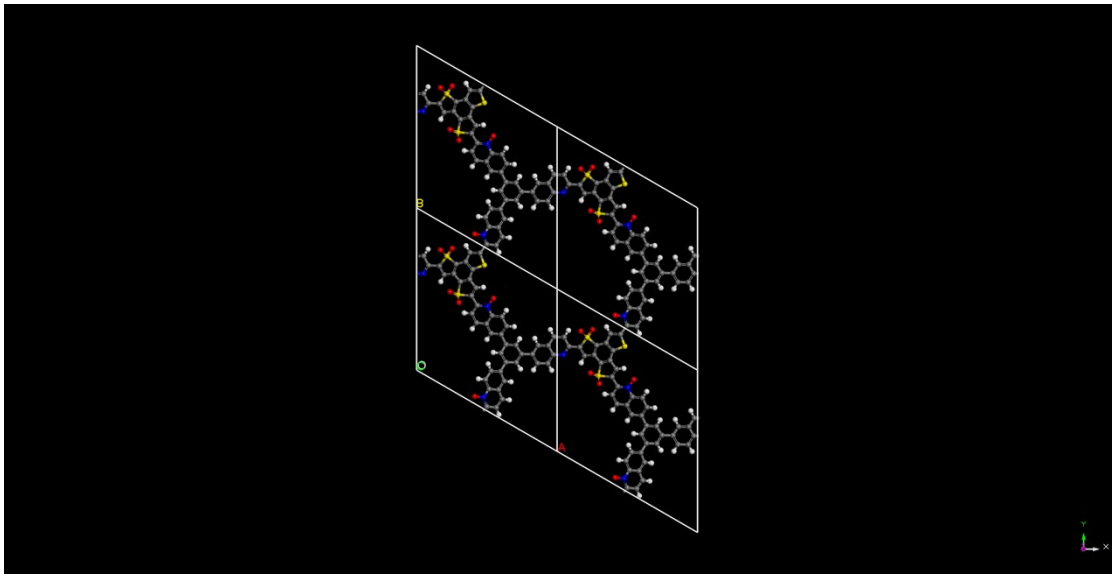

Fig. S2 AA-stacking structure of NQ-COF_{S1}-O.

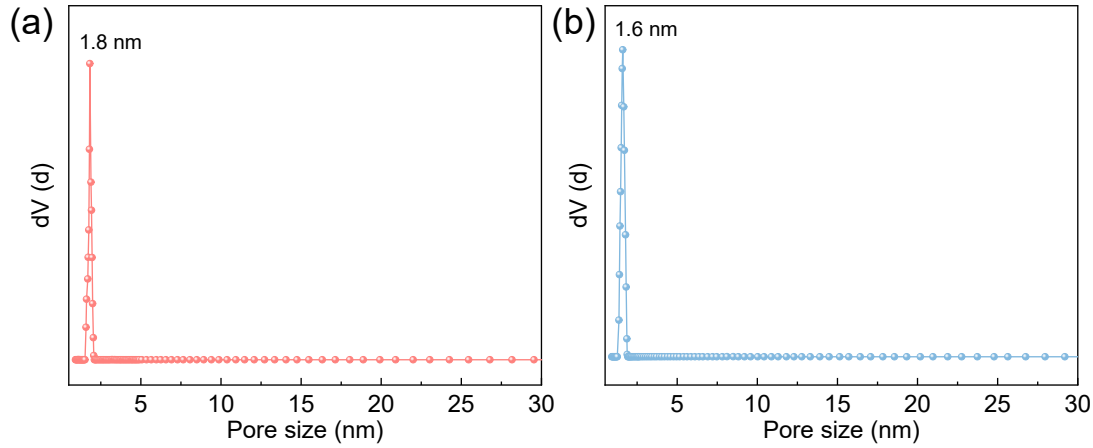

Fig. S3 Pore size distribution plots of (a) NQ-COF_{S1} and (b) NQ-COF_{S1}-O.

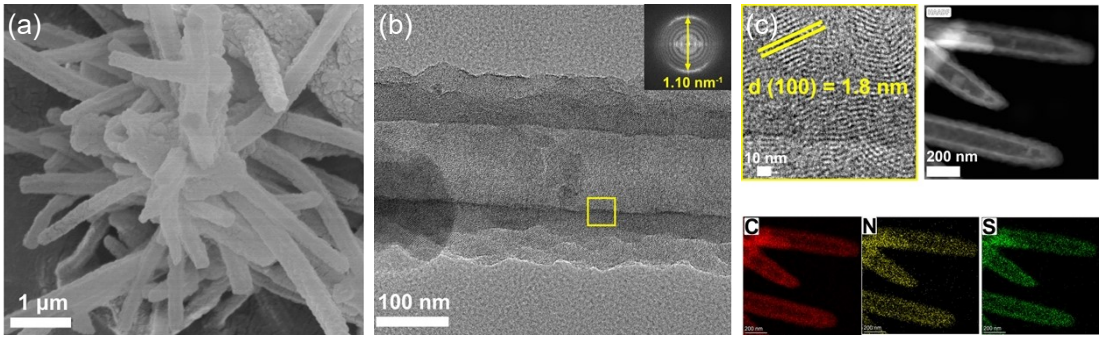

Fig. S4 a) SEM and b) TEM images of NQ-COF_{S1}. c) Partial enlargement of b) and elemental mapping images of NQ-COF_{S1}.

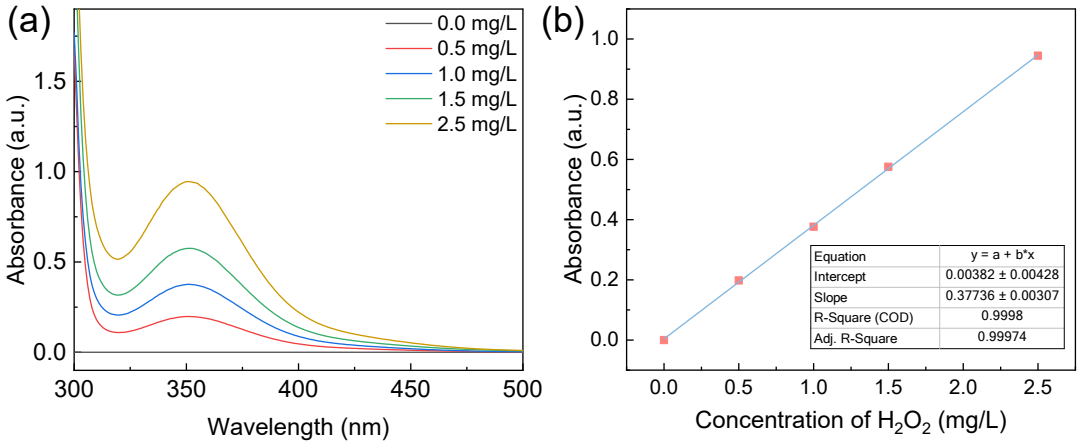

Fig. S5 a) The absorption spectra of H_2O_2 with different concentrations at wavelengths of 300-500 nm. b) The corresponding standard curve.

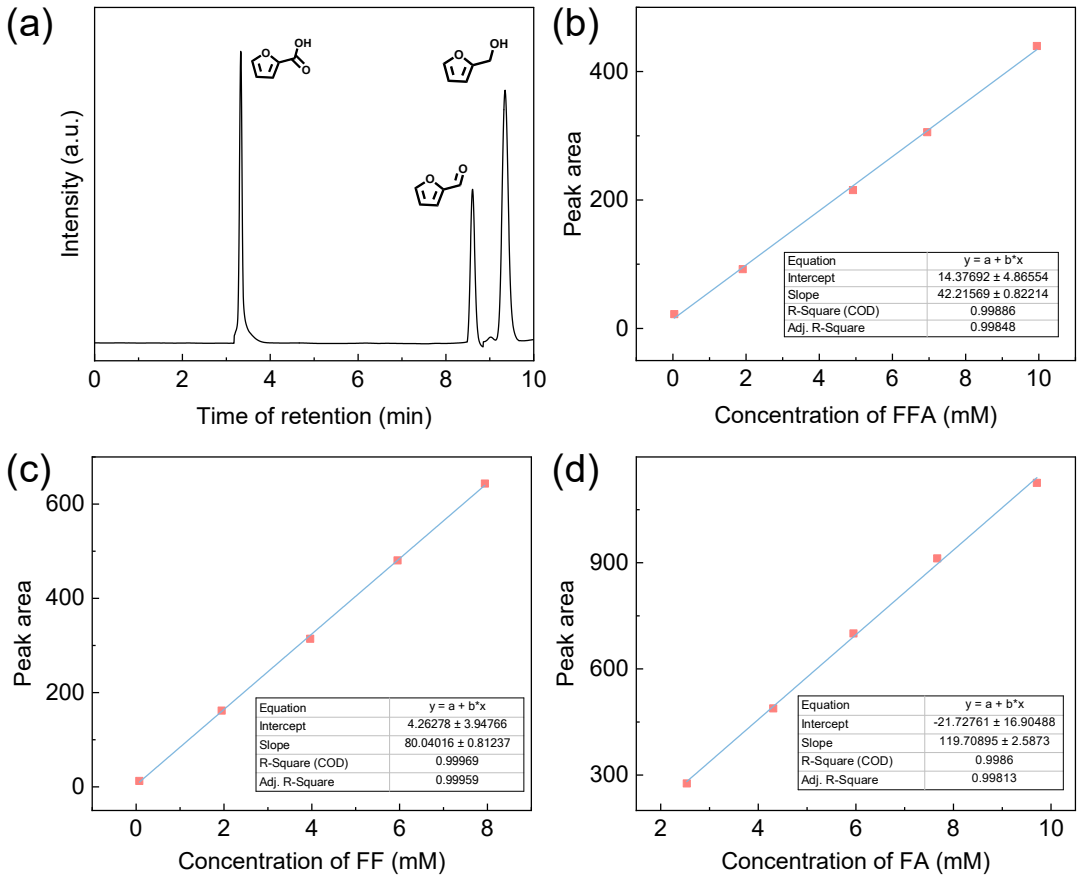

Fig. S6 a) HPLC spectra of FFA, FF, and FA standards. The standard curves of b) FFA, c) FF, and d) FA.

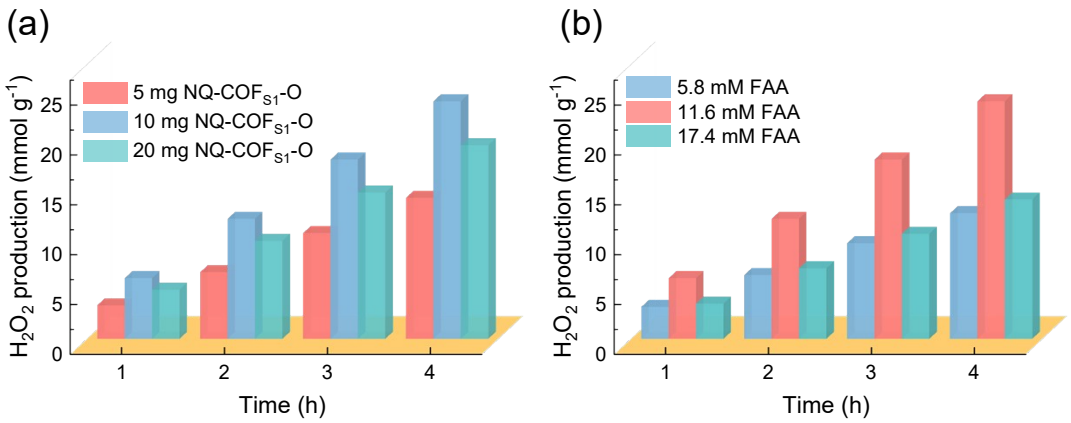

Fig. S7 a) Photocatalytic H_2O_2 production in 11.6 mM FFA solution with different dosages of NQ-COF_{S1}-O. b) Photocatalytic H_2O_2 production in different concentration of FFA solutions with 10 mg of NQ-COF_{S1}-O.

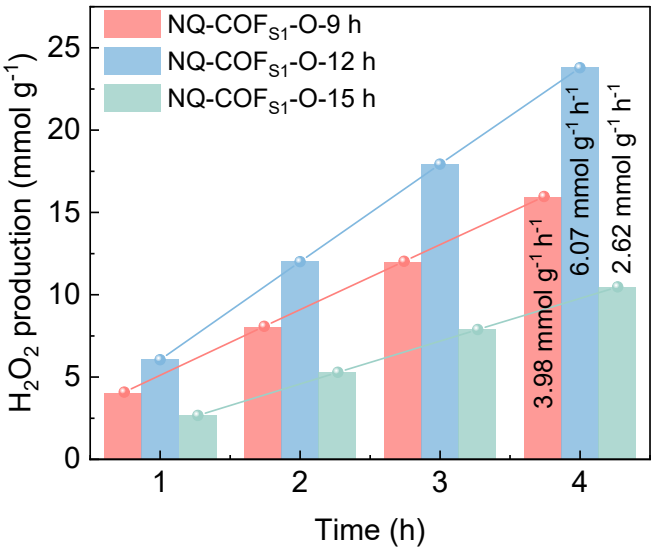

Fig. S8 Photocatalytic H_2O_2 production in 11.6 mM FFA solution over NQ-COF$_{S1}$-O with different oxidation degrees. Note that NQ-COF$_{S1}$-O with varying degrees of oxidation were prepared by adjusting the oxidation reaction time (9, 12, and 15 hours), yielding the samples labeled as NQ-COF$_{S1}$-O-9h, NQ-COF$_{S1}$-O-12h, and NQ-COF$_{S1}$-O-15h, respectively

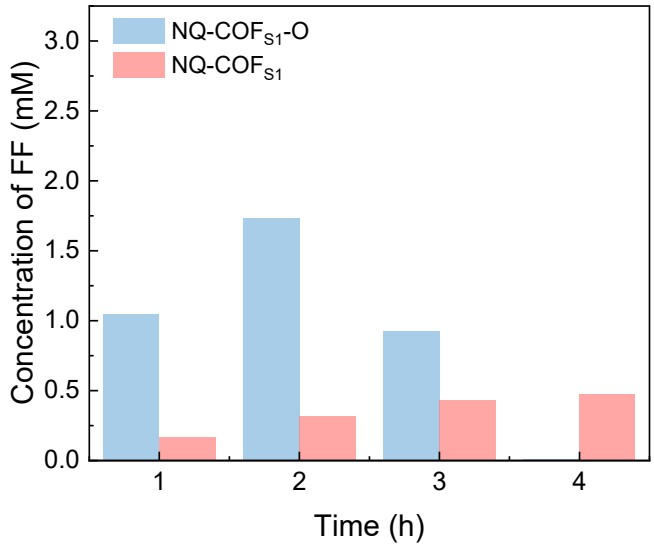

Fig. S9 Photocatalytic FF production over NQ-COF$_{S1}$ and NQ-COF$_{S1}$-O in 11.6 mM FFA solution.

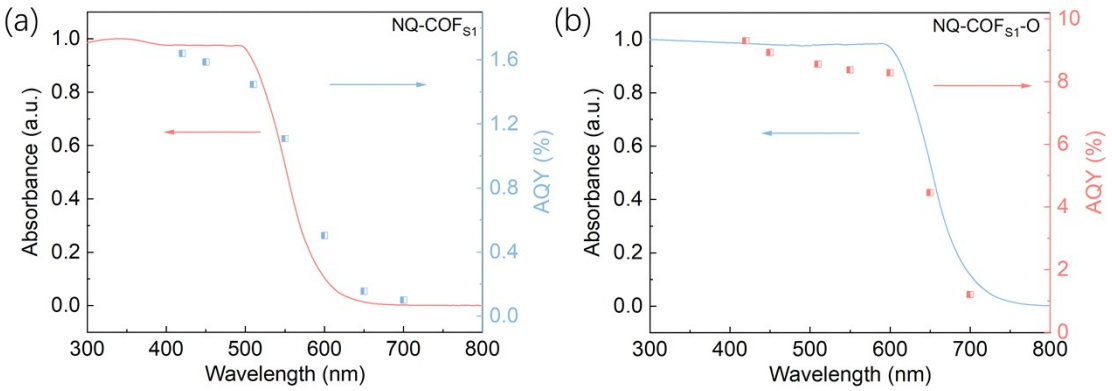

Fig. S10 Wavelength-dependent H_2O_2 apparent quantum yield (AQY) on (a) NQ-COF_{S1} and (b) NQ-COF_{S1}-O.

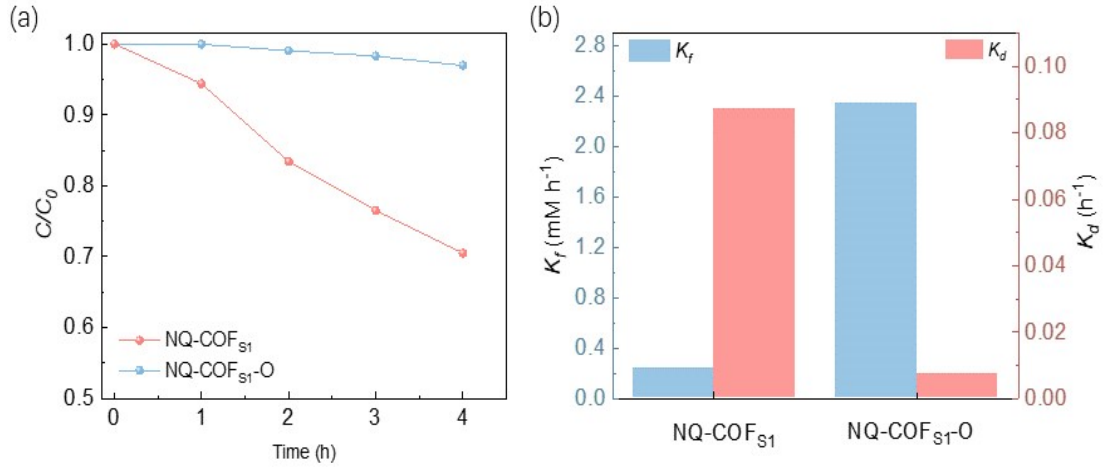

Fig. S11 a) H_2O_2 decomposition curves under light irradiation. b) H_2O_2 formation rate constant (K_f) and decomposition rate constant (K_d).

The kinetic parameters, specifically the first-order kinetics formation rate constant (K_f) and the zero-order kinetics decomposition rate constant (K_d), are calculated by analyzing the H_2O_2 formation and decomposition data. The values of K_f and K_d are estimated by the equation as follows:

$$[\mathrm{H2O2}] = \frac{K_f}{K_d} \times (1 - e^{-K_d t})$$

$$K_d = \frac{-\ln(c_t/c_0)}{t}$$

Where c_t and c_0 are the H_2O_2 concentration at t and initial time, respectively.

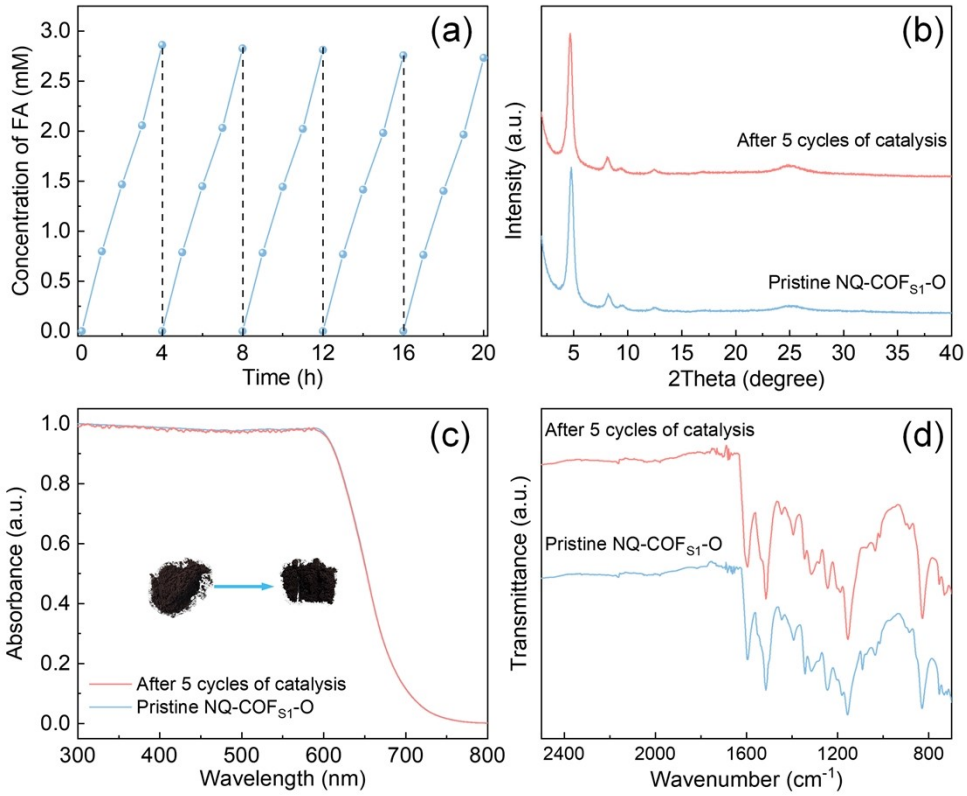

Fig. S12 a) Recycling FA production over NQ-COF$_{S1}$-O. b) PXRD patterns, c) UV-vis DRS spectra, and d) FT-IR spectra of NQ-COF$_{S1}$-O before and after five cycles of photocatalysis.

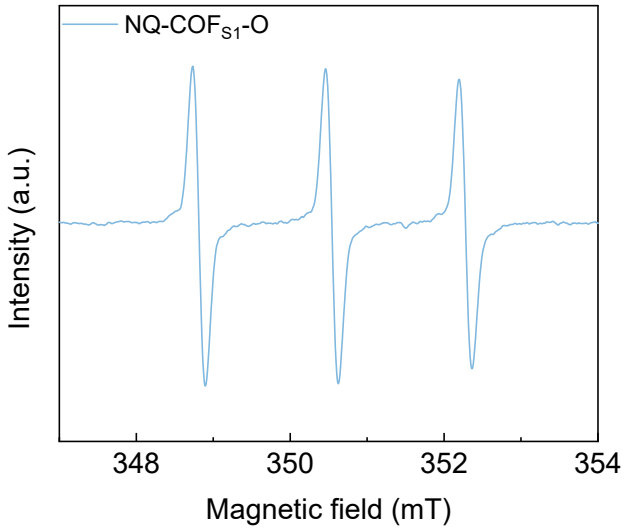

Fig. S13 $^1O_2$ trapped by TEMP over NQ-COF$_{S1}$-O under light.

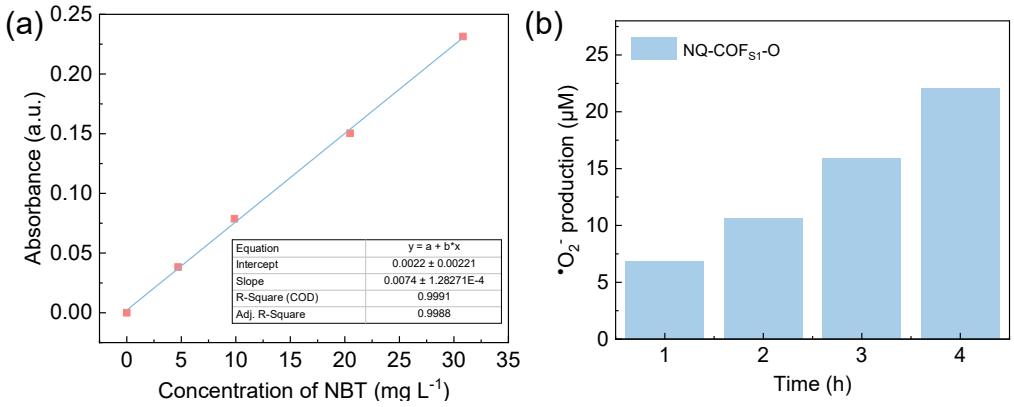

Fig. S14 Quantitative measurement of $^{\bullet}O_2^-$.

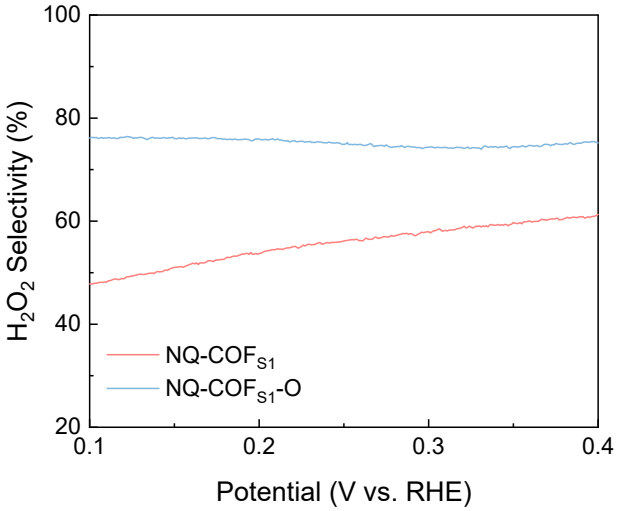

Fig. S15 The dependence of H_2O_2 selectivity on the potential.

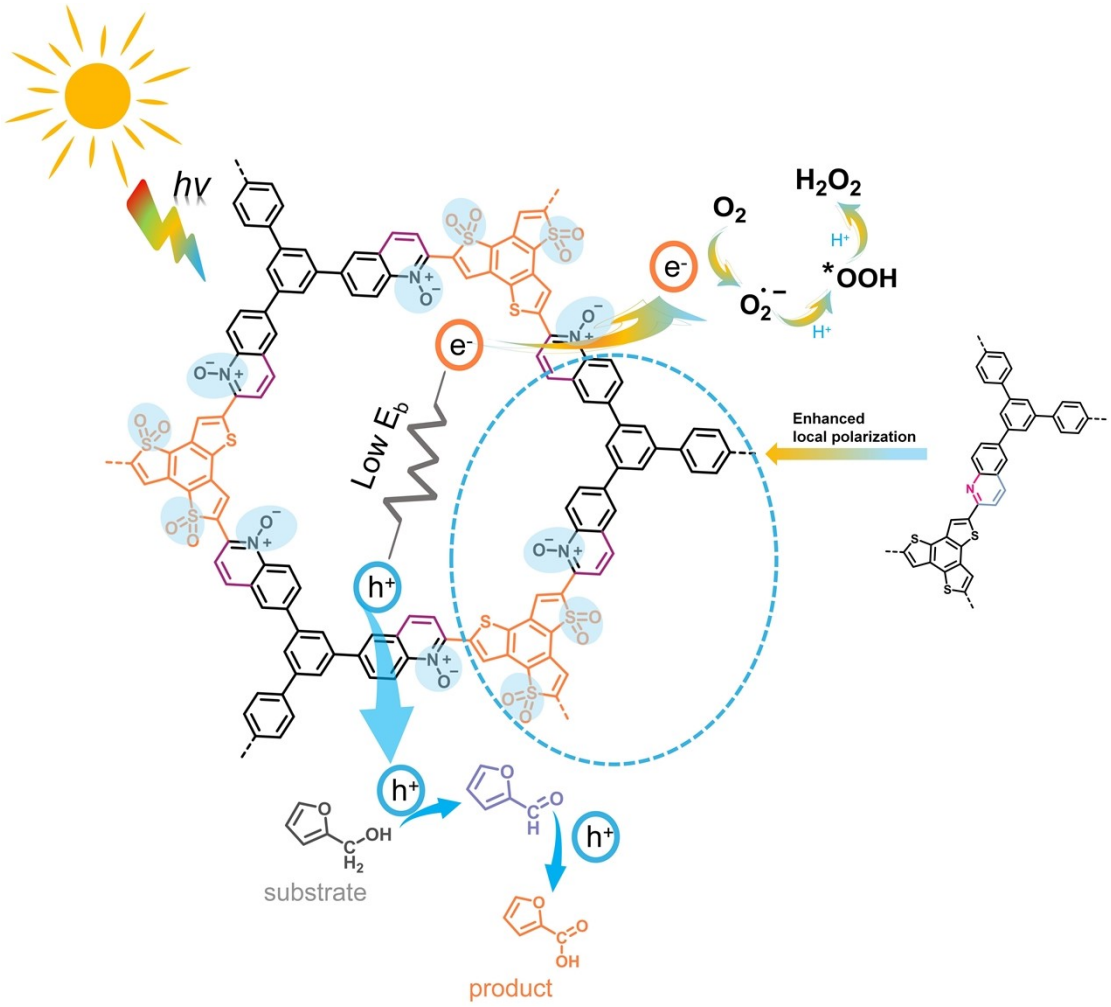

Fig. S16 Proposed mechanism of photocatalytic H_2O_2 production and FFA oxidation by NQ-COF_{S1}-O.

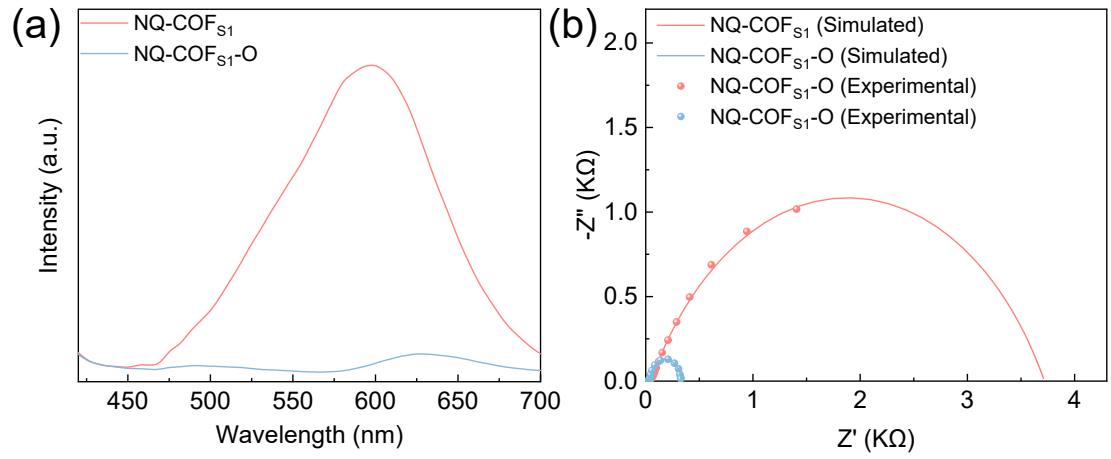

Fig. S17 a) PL spectra and b) Nyquist plots of NQ-COF_{S1} and NQ-COF_{S1}-O.

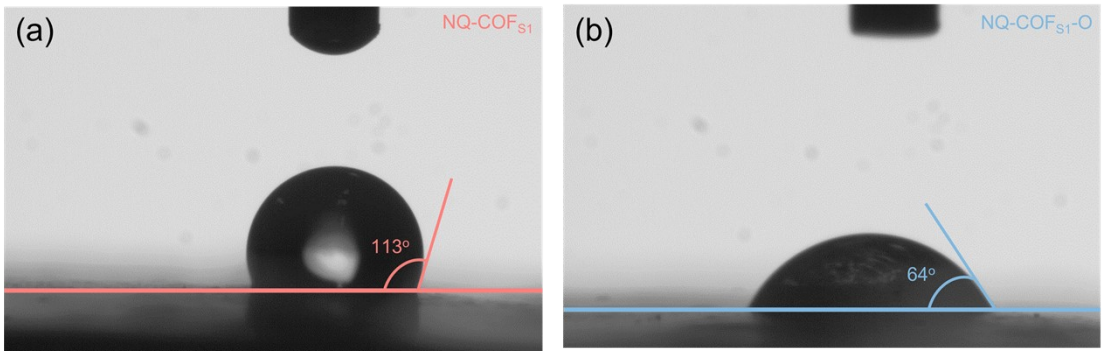

Fig. S18 Water contact angles of a) NQ-COF$_{S1}$ and b) NQ-COF$_{S1}$-O.

Table S1 Atomistic coordinates of AA stacking for NQ-COF$_{S1}$ optimized by using Materials Studio method.

Atom	*x/a*	*y/b*	*z/c*
C1	0.28623	0.79233	-0.73856
C2	0.26749	0.72254	-0.79883
C3	0.31925	0.70280	-0.81046
C4	0.38926	0.75344	-0.75722
C5	0.40864	0.82427	-0.69568
C6	0.35726	0.84336	-0.68971
S7	0.49226	0.89301	-0.63144
C8	0.45742	0.94837	-0.60228
C9	0.38486	0.91435	-0.63713
S10	0.21703	0.80715	-0.72380
C11	0.16164	0.71781	-0.79709
C12	0.19616	0.67959	-0.83551
S13	0.30507	0.61958	-0.88456
C14	0.39479	0.65342	-0.84337
C15	0.43274	0.72545	-0.77505
C16	0.08398	0.68442	-0.80459
N17	0.04392	0.61630	-0.92276
C18	0.60026	0.40634	-0.72046
C19	0.63352	0.36567	-0.73916
C20	0.70656	0.40039	-0.80503
C21	0.74527	0.47377	-0.86827
C22	0.70886	0.51143	-0.88360
C23	0.63689	0.47879	-0.80102
C24	0.60010	0.52045	-0.79612
C25	0.59116	0.28707	-0.70269
C26	0.82370	0.51193	-0.90269
C27	0.63507	0.59095	-0.67050
C28	0.60070	0.63023	-0.66490
C29	0.53081	0.59960	-0.77937

C30	0.49477	0.52890	-0.90289
C31	0.52964	0.48994	-0.91436
C32	0.85942	0.47819	-1.04287
C33	0.93313	0.51318	-1.04915
C34	0.97234	0.58271	-0.92326
C35	0.93746	0.61797	-0.79419
C36	0.86389	0.58241	-0.77936
C37	0.52049	0.25053	-0.82354
C38	0.48069	0.17698	-0.80559
C39	0.51103	0.13824	-0.67792
C40	0.58172	0.17334	-0.55858
C41	0.62106	0.24747	-0.56468
C42	0.42865	0.60961	-0.87000
N43	0.49729	0.63764	-0.76729
C44	0.50089	0.02606	-0.57212
N45	0.47293	0.06659	-0.67951
C46	0.57107	1.05899	-0.45042
C47	0.61137	1.13282	-0.44094
C48	1.05071	1.72150	-1.68259
C49	0.97742	1.68807	-1.67583
C50	1.39110	1.53930	-2.99425
C51	1.42434	1.49900	-3.01185
H52	0.35405	0.94053	-0.62949
H53	0.17026	0.62310	-0.88022
H54	0.48931	0.75577	-0.74067
H55	0.54567	0.38170	-0.63828
H56	0.73333	0.37036	-0.80664
H57	0.73651	0.56647	-0.96309
H58	0.68852	0.61525	-0.56771
H59	0.62777	0.68412	-0.56471
H60	0.50227	0.43647	-1.02065
H61	0.83069	0.42513	-1.15294
H62	0.95994	0.48664	-1.15570
H63	0.83848	0.60918	-0.65817
H64	0.49635	0.27842	-0.94604
H65	0.42688	0.14962	-0.90415
H66	0.67444	0.27375	-0.46068
H67	0.59402	1.02762	-0.36120
H68	0.66538	1.15802	-0.34528
H69	1.08113	1.77533	-1.58424
H70	0.95212	1.71647	-1.57369
H71	1.33675	1.51621	-3.08065
H72	1.39534	1.44502	-3.11084

Table S2 Atomistic coordinates of AA stacking for NQ-COF_{S1}-O optimized by using Materials Studio method.

Atom	*x/a*	*y/b*	*z/c*
C1	0.27999	0.79261	-0.65600
C2	0.26295	0.72456	-0.76087
C3	0.31040	0.69948	-0.68408
C4	0.37642	0.74702	-0.54778
C5	0.39702	0.81879	-0.49171
C6	0.34884	0.84115	-0.54901
S7	0.48107	0.88667	-0.41276
C8	0.45062	0.94571	-0.46383
C9	0.37886	0.91319	-0.53446
S10	0.21441	0.80837	-0.84083
C11	0.16175	0.72185	-1.03719
C12	0.19449	0.68499	-0.96457
S13	0.29334	0.61107	-0.82907
C14	0.39014	0.65261	-0.69990
C15	0.42091	0.71700	-0.54699
C16	0.08383	0.68708	-1.08826
N17	0.04384	0.61510	-1.10538
C18	0.59973	0.40427	-0.74069
C19	0.63523	0.36552	-0.69853
C20	0.70885	0.40115	-0.76390
C21	0.74537	0.47122	-0.89820
C22	0.70690	0.50626	-0.95192
C23	0.63566	0.47535	-0.85249
C24	0.60075	0.51933	-0.84543
C25	0.59556	0.28832	-0.58994
C26	0.82365	0.50895	-0.97229
C27	0.63918	0.59033	-0.73083
C28	0.60698	0.63167	-0.70563
C29	0.53508	0.60313	-0.78702
C30	0.49634	0.53220	-0.90503
C31	0.52907	0.49096	-0.93702
C32	0.85924	0.47150	-1.05176
C33	0.93280	0.50708	-1.09997
C34	0.97200	0.58065	-1.08270
C35	0.93695	0.61906	-1.02589
C36	0.86402	0.58348	-0.96128
C37	0.52935	0.25854	-0.41134
C38	0.48960	0.18599	-0.33920
C39	0.51486	0.14060	-0.43625
C40	0.58213	0.16961	-0.60186

C41	0.62155	0.24247	-0.68047
C42	0.43093	0.61406	-0.79697
N43	0.50288	0.64304	-0.74803
C44	0.49800	0.02398	-0.48260
N45	0.47514	0.06930	-0.37240
C46	0.56578	1.05179	-0.63590
C47	0.60777	1.12442	-0.69471
C48	1.04959	1.72679	-2.06561
C49	0.97632	1.69280	-2.02764
C50	1.39309	1.54439	-2.93886
C51	1.42536	1.50398	-2.99064
H52	0.35072	0.94117	-0.59541
H53	0.17038	0.62901	-1.02227
H54	0.47389	0.74655	-0.44129
H55	0.54413	0.37999	-0.68314
H56	0.73819	0.37502	-0.69933
H57	0.73190	0.55825	-1.07372
H58	0.69390	0.61359	-0.64878
H59	0.63740	0.68576	-0.61115
H60	0.49877	0.43709	-1.03458
H61	0.83061	0.41467	-1.07749
H62	0.95969	0.47768	-1.15022
H63	0.83995	0.61462	-0.89018
H64	0.50797	0.29092	-0.31817
H65	0.43868	0.16454	-0.20544
H66	0.67086	0.26216	-0.82771
H67	0.58452	1.01671	-0.72468
H68	0.65904	1.14483	-0.82377
H69	1.07988	1.78394	-2.06208
H70	0.95081	1.72399	-1.99303
H71	1.33772	1.51996	-3.00657
H72	1.39446	1.45040	-3.09313
O73	0.41170	1.04299	0.81224
O74	0.25143	0.87496	-0.08552
O75	0.16750	0.82305	0.42004
O76	0.23577	0.59886	0.45696
O77	0.29953	0.56479	0.47286
O78	0.54545	0.71399	0.32097

Table S3 Comparison of H_2O_2 production performance for different COF photocatalysts reported in the literatures.

Entry	COFs	Reaction medium	Irradiation (nm)	H_2O_2 yield (μmol h^{-1} g^{-1})	AQY	SCC	Ref
1	TF_{50}-COF (5 mg)	H_2O: EtOH (9: 1) (50 mL)	λ > 400 300 W Xe lamp	1739	5.1% at 400 nm	0.17 at AM 1.5G	1]
2	TTF-BT-COF (50 mg)	H_2O (100 mL)	λ > 420 300 W Xe lamp	2760	11.19% at 420 nm	0.49 at 420 nm	2
3	TPB-DMTP-COF (10 mg)	H_2O (50 mL)	λ > 420 300 W Xe lamp	1565	18.4% at 420 nm	0.76% at AM 1.5G	3
4	Py-Da-COF (5 mg)	H_2O: BA (9: 1) (5 mL)	λ > 420 300 W Xe lamp	1242	4.5% at 420 nm	0.09% at AM 1.5G	4
5	HEP-TAPT-COF (50 mg)	H_2O (100 mL)	λ > 420 300 W Xe lamp	1750	15.35% at 420 nm	0.65% at AM 1.5G	5
6	Bpy-TAPT (5 mg)	H_2O (30 mL)	λ > 420 300 W Xe lamp	4038	8.6% at 420 nm	0.65% at AM 1.5G	6
7	TDB-COF (10 mg)	H_2O (10 mL)	AM 1.5G 300 W Xe lamp	723	1.4% at 365 nm	0.39% at AM 1.5G	7
8	CHF-DPDA (40 mg)	H_2O (20 mL)	λ > 420 300 W Xe lamp	1725	16% at 420 nm	0.78% at AM 1.5G	8
9	Cu_3-BT-COF (5 mg)	11.6 mM FFA	300 W Xe lamp	1168	7.98% at 420 nm	0.62% at 420 nm	9
10	COF-TfpBpy (15 mg)	H_2O (10 mL)	λ > 420 300 W Xe lamp	2084	13.6% at 420 nm	1.08% at 420 nm	10
11	TaptBtt (15 mg)	H_2O (50 mL)	λ > 420 300 W Xe lamp	1407	4.6% at 450 nm	0.296% at AM 1.5G	11
12	TpDz (3 mg)	H_2O (18 mL)	λ > 420 300 W Xe lamp	7327	11.9% at 420 nm	0.62% at λ > 420 nm	12
13	TAPT-TFPA COFs@Pd ICs (10 mg)	H_2O: EtOH (9: 1) (20 mL)	AM 1.5G 300 W Xe lamp	2143	6.5% at 400 nm	0.82% at AM 1.5G	13
14	TZ-COF (15 mg)	H_2O: BA (1: 1) (30 mL)	λ > 420 300 W Xe lamp	4951	0.6% at 475 nm	0.036% at AM 1.5G	14
15	COF-N32 (10 mg)	H_2O (50 mL)	λ > 420 300 W Xe lamp	605	6.2% at 459 nm	0.31% at 300 W Xe lamp	15
16	CTF-BDDBN (30 mg)	H_2O (50 mL)	λ > 420 300 W Xe lamp	997	-	0.14% at AM 1.5G	16
17	Kf-AQ (5 mg)	Alkaline water (pH = 13, 30 mL)	λ > 400 300 W Xe lamp	4784	15.8% at 400 nm	0.7% at 400 nm	17

18	DVA-COF (10 mg)	H_2O: BA (9: 1) (20 mL)	420 nm LED	8450	2.84% at 420 nm	0.08% at AM 1.5G	18
19	TAH-COF (5 mg)	H_2O (50 mL)	λ > 420 300 W Xe lamp	6003	7.72% at 500 nm	0.66% at AM 1.5G	19
20	*o*-COF-TpPzda (5 mg)	H_2O (40 mL)	λ > 420 300 W Xe lamp	4396	-	0.46%	20
21	TB-COF (1 mg)	Seawater (8 mL)	400-700 nm white LED	4111	3.45% at 420 nm	1.08% at 400-700 nm white LED	21
22	FS-OHOMe-COF (10 mg)	H_2O (20 mL)	λ > 420 300 W Xe lamp	10000	9.6% at 420 nm	0.58% at AM 1.5G	22
23	SO_3H-COF (5 mg)	H_2O: EtOH (9: 1) (50 mL)	λ > 400 300 W Xe lamp	4971	15% at 400 nm	0.4% at AM 1.5G	23
24	Fe SAS-TpPP-COF (5 mg)	H_2O: EtOH (9: 1) (50 mL)	λ > 420 300 W Xe lamp	4130	6.4% at 420 nm	0.2% at AM 1.5G	24
25	Tz-THBZ (10 mg)	H_2O (50 mL)	λ > 420 300 W Xe lamp	4688	5.5% at 420 nm	0.36% at AM 1.5G	25
26	NQ-COF_{S1}-O (10 mg)	11.6 mM FFA	λ > 420 300 W Xe lamp	6070	9.2% at 420 nm	0.61% at 420 nm	This work

4. References

1 H. Wang, C. Yang, F. Chen, G. Zheng and Q. Han, *Angew. Chem. Int. Ed.*, 2022, **61**, e202202328.

2 J. N. Chang, Q. Li, J. W. Shi, M. Zhang, L. Zhang, S. Li, Y. Chen, S. L. Li and Y. Q. Lan, *Angew. Chem. Int. Ed.*, 2023, **62**, e202218868.

3 L. Li, L. Xu, Z. Hu and J. C. Yu, *Adv. Funct. Mater.*, 2021, **31**, 2106120.

4 J. Sun, H. Sekhar Jena, C. Krishnaraj, K. Singh Rawat, S. Abednatanzi, J. Chakraborty, A. Laemont, W. Liu, H. Chen, Y. Y. Liu, K. Leus, H. Vrielinck, V. Van Speybroeck and P. Van Der Voort, *Angew. Chem. Int. Ed.*, 2023, **62**, e202216719.

5 D. Chen, W. Chen, Y. Wu, L. Wang, X. Wu, H. Xu and L. Chen, *Angew. Chem. Int. Ed.*, 2023, **62**, e202217479.

6 Y. Liu, W.-K. Han, W. Chi, Y. Mao, Y. Jiang, X. Yan and Z.-G. Gu, *Appl. Catal. B Environ.*, 2023, **331**, 122691.

7 Z. Zhou, M. Sun, Y. Zhu, P. Li, Y. Zhang, M. Wang and Y. Shen, *Appl. Catal. B Environ.,* 2023, **334**, 122862.

8 H. Cheng, H. Lv, J. Cheng, L. Wang, X. Wu and H. Xu, *Adv. Mater.*, 2022, **34**, 2107480.

9 J. N. Chang, J. W. Shi, Q. Li, S. Li, Y. R. Wang, Y. Chen, F. Yu, S. L. Li and Y. Q. Lan, *Angew. Chem. Int. Ed.*, 2023, **62**, e202303606.

10 M. Kou, Y. Wang, Y. Xu, L. Ye, Y. Huang, B. Jia, H. Li, J. Ren, Y. Deng, J. Chen, Y. Zhou, K. Lei, L. Wang, W. Liu, H. Huang and T. Ma, *Angew. Chem. Int. Ed.*,

2022, **61**, e202200413.

11 C. Qin, X. Wu, L. Tang, X. Chen, M. Li, Y. Mou, B. Su, S. Wang, C. Feng, J. Liu, X. Yuan and Y. Zhao, H. Wang, *Nat. Commun.*, 2023, **14**, 5238.

12 Q. Liao, Q. Sun, H. Xu, Y. Wang, Y. Xu, Z. Li, J. Hu, D. Wang, H. Li and K. Xi, *Angew. Chem. Int. Ed.*, 2023, **62**, e202310556.

13 Y. Liu, L. Li, H. Tan, N. Ye, Y. Gu, S. Zhao, S. Zhang, M. Luo and S. Guo, *J. Am. Chem. Soc.*, 2023, **145**, 19877-19884.

14 Y. Mou, X. Wu, C. Qin, J. Chen, Y. Zhao, L. Jiang, C. Zhang, X. Yuan, E. H. Ang and H. Wang, *Angew. Chem. Int. Ed.*, 2023, **62**, e202309480.

15 F. Liu, P. Zhou, Y. Hou, H. Tan, Y. Liang, J. Liang, Q. Zhang, S. Guo, M. Tong and J. Ni, *Nat. Commun.*, 2023, **14**, 4344.

16 L. Chen, L. Wang, Y. Wan, Y. Zhang, Z. Qi, X. Wu and H. Xu, *Adv. Mater.*, 2020, **32**, 1904433.

17 X. Zhang, S. Cheng, C. Chen, X. Wen, J. Miao, B. Zhou, M. Long and L. Zhang, *Nat. Commun.*, 2024, **15**, 2649.

18 H. Yu, F. Zhang, Q. Chen, P.-K. Zhou, W. Xing, S. Wang, G. Zhang, Y. Jiang and X. Chen, *Angew. Chem. Int. Ed.*, 2024, **63**, e202402297.

19 T. Xu, Z. Wang, W. Zhang, S. An, L. Wei, S. Guo, Y. Huang, S. Jiang, M. Zhu, Y.-B. Zhang and W.-H. Zhu, *J. Am. Chem. Soc.*, 2024, **146**, 20107-20115.

20 T. Yang, D. Zhang, A. Kong, Y. Zou, L. Yuan, C. Liu, S. Luo, G. Wei and C. Yu, *Angew. Chem. Int. Ed.*, 2024, **63**, e202404077.

21 J.-Y. Yue, L.-P. Song, Z.-X. Pan, P. Yang, Y. Ma, Q. Xu and B. Tang, *ACS Catal.*,

2024, **14**, 4728-4737.

22 C. Shu, X. Yang, L. Liu, X. Hu, R. Sun, X. Yang, A. I. Cooper, B. Tan and X. Wang, *Angew. Chem. Int. Ed.*, 2024, **63**, e202403926.

23 L. Li, X. Lv, Y. Xue, H. Shao, G. Zheng and Q. Han, *Angew. Chem. Int. Ed.*, 2024, **63**, e202320218.

24 Z. Li, X. Shi, H. Cheng, Y. Song, Y. Jiao, S. Shi, J. Gao and J. Hou, *Adv. Energy Mater.*, 2024, **14**, 2302797.

25 C. Shu, P. Xie, X. Yang, X. Yang, H. Gao, B. Tan and X. Wang, *J. Mater. Chem. A.*, 2024, **12**, 25927-25933.